




Cite this: *Nanoscale*, 2023, 15, 8754

Operando surface optical nanometrology reveals diazonium salts' visible photografting mechanism†

Baptiste Maillot, Madelyn Johnson, Jean-Frédéric Audibert, Fabien Miomandre  and Vitor Brasiliense *

High resolution and quantitative surface modification through photografting is a highly desirable strategy towards the preparation of smart surfaces, enabling chemical functions to be precisely located onto specific regions of inert surfaces. Although promising, the mechanisms leading to direct (without the use of any additive) photoactivation of diazonium salts using visible wavelengths are poorly understood, precluding the generalization of popular diazonium-based electrografting strategies into high resolution photografting ones. In this paper, we employ quantitative phase imaging as a nanometrology tool for evaluating the local grafting rate with diffraction-limited resolution and nanometric precision. By carefully measuring the surface modification kinetics under a range of different conditions, we reveal the reaction mechanism while evaluating the influence of key parameters, such as the power density, the radical precursor concentration and the presence of side reactions.

Received 30th January 2023,

Accepted 6th April 2023

DOI: 10.1039/d3nr00439b

rsc.li/nanoscale

Introduction

Local and controlled surface modification constitute an interesting strategy for preparing smart functional surfaces,^{1–4} enabling the implementation of chemical functions (sensors,¹ anti-biofouling,⁵ protein anchoring,^{3,6} catalysts,⁴ *etc.*) with minimal usage of precursors. Ideally, a surface modification procedure should be triggered locally with high resolution, be carried out in green solvents such as water, and enable a large span of chemical groups to be added to a variety of surfaces. Radical based processes offer several of these characteristics,^{7–9} owing to the reactivity of intermediate species. Among several available radical precursors, aryldiazonium salts are particularly popular ones, owing to their easiness of activation and preparation from anilines.^{10,11}

Diazonium-based strategies have been shown to enable the modification of a large variety of surfaces, including metals,^{12,13} semiconductors,^{10,14} carbon-based materials^{15,16} and even insulating surfaces.^{17,18} When no spatial resolution is required, grafting over conductive surfaces remains the most popular usage of these molecules, as cleavage of the N₂ leaving group can be conveniently activated through electrochemical reduction. In situations where spatial resolution is sought, however, methodologies for activating grafting reactions are much rarer. For instance, local probes can be used to locally

reduce the diazonium salts, or to locally deliver them (or a precursor),^{19–22} but these strategies remain relatively difficult to implement and suffer from low throughput. Photochemical routes are extremely promising in this regard, as high resolution can be straightforwardly achieved with relatively simple optical elements, while remaining fast, reproducible and scalable. Diazonium salts, however, rarely exhibit absorption bands in the visible range, and consequently it was believed until recently that photografting of diazonium salts requires special conditions to take place, such as UV stimulation, the formation of charge transfer complexes,¹² sensitizers^{23,24} or other external reaction triggers, such as plasmonic entities.^{25–29}

Our group has recently shown that controlled photografting of diazonium salts is possible using only visible light in aqueous media without the presence of any additive or special conditions.¹⁷ Such simplicity, associated with the ability to manipulate optical fields, enables sub-micrometric range patterning with relatively modest instrumentation (a visible laser and a microscope). Pursuing such applications, however, requires a better understanding of the photochemically driven grafting process, insight into the reaction mechanism, and identifying its main controlling parameters. In spite of its popularity, quantitative studies of diazonium grafting kinetics are scarce, and the existing examples deal with electrochemical^{30,31} or spontaneous grafting.^{32,33} Since such grafting strategies strongly depend on the surface characteristics, their kinetics rather reveal the evolution of the surface properties and therefore does not generalize to the photografting situation.

Université Paris-Saclay, ENS Paris-Saclay, CNRS, PPSM, 4 avenue des sciences, 91190 Gif-sur-Yvette, France. E-mail: vitor.brasiliense@ens-paris-saclay.fr

† Electronic supplementary information (ESI) available. See DOI: <https://doi.org/10.1039/d3nr00439b>



In this paper, we investigate the direct photografting of diazonium salts using diffuser-based phase sensing and imaging (DIPSi), a recently introduced quantitative phase imaging implementation^{17,34,45} which allows tracking of the optical thickness of the growing grafting layers *in situ* with diffraction-limited resolution and nanometric precision.¹⁷ By measuring the grafting kinetics carried out at different power densities, concentrations, and excitation wavelengths and in the presence of additives, we quantitatively investigate the mechanisms involved in the photografting reaction and identify routes to control it. In particular, we gather insight into the flexibilization of wavelength absorption criteria and explain why the reaction can be triggered in the visible range, while no clear absorption peak seems to exist at such wavelengths.

Besides consolidating the use of quantitative phase imaging strategies as a chemical metrology tool for tracking surface modification kinetics, this work will set the basis for a wider utilisation of diazonium salts through photochemical routes, a considerable extension of this very popular surface functionalization reaction. Considering the extensive use of diazonium electrografting for functionalizing whole conductive surfaces, we can reasonably expect that the understanding of direct photografting derived from our work could support and enable a correspondingly widespread usage of this reaction with high spatial control.

Experimental

Materials and methods

Grafting solutions were prepared from 4-nitrobenzenediazonium tetrafluoroborate (Sigma Aldrich, 96%) dissolved in Milli-Q water ($18.2 \text{ M}\Omega \text{ cm}^{-1}$), the pH of which was adjusted to 2 using a 1 M hydrochloric acid solution (Sigma Aldrich). Solutions containing (2,2,6,6-tetramethylpiperidin-1-yl)oxy

(Sigma Aldrich) were prepared in a 1:1 solvent mixture of Milli-Q water at pH 2 and dimethylsulfoxide (Carlo Erba Reagents). *m*-Methyl-diazonium chloride used in control experiments was prepared from *m*-toluidine (99%, Sigma Aldrich) using sodium nitrite (Acros Organics) aqueous solution (pH 2) at stoichiometric proportions. All commercial chemicals were used without further purification.

Grafting setup

All grafting experiments were conducted on an inverted microscope (Nikon Eclipse Ti), using a 100 \times oil immersion (Nikon, NA = 1.49), a 1.5 \times tube lens and a 2.5 \times relay lens system (C-Mount TV Relay Lens VM 2.5 \times) to achieve a total 375 \times magnification. An excitation laser is introduced through the backport of the microscope, and focused onto the grafting surface, as indicated in Fig. 1A. The grafting solution is kept in a 10 μm thin cell (Hellma). The relation between the optical path difference (OPD) and the actual object thickness (L) is given by $\text{OPD} = \Delta n \times L$, where Δn is the refractive index difference between the growing layer and the medium. In our setup, we typically observe sub-nanometric noise (typically 0.3–0.5 nm for 1 Hz acquisition rate), which allows quantification of thin polymeric layers as long as a significant refractive index difference exists. Indicatively, for a 10 nm thin layer, polymers differing from the solution refractive index by more than 0.03–0.05 would thus be detectable. Due to the need to vary both the laser power and radical precursor concentration over several orders of magnitude, it was essential that we were able to assess grafting kinetics at widely different timescales (ms to min). Triggering each laser impulsion, as done previously,¹⁷ becomes impractical in such conditions, as low fluency experiments would require unreasonably long experiment times. Instead, here we employ a simpler illumination scheme, using a precision shutter (Edmund Optics) to block

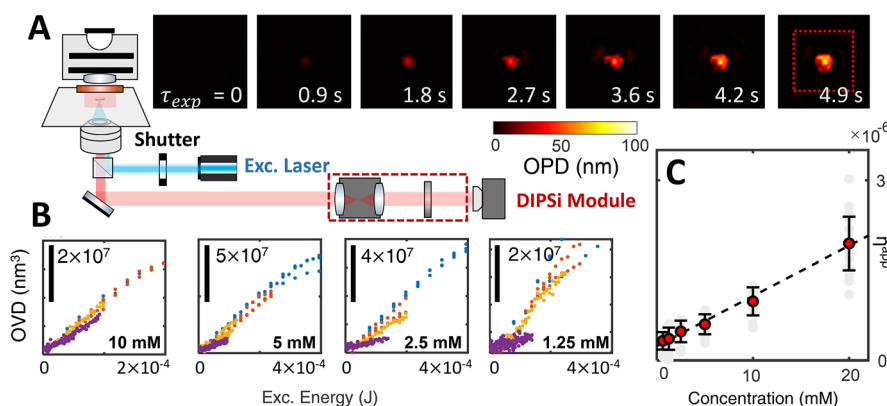


Fig. 1 (A) Experimental setup and typical sequence of OPD images ($5.2 \times 5.2 \mu\text{m}^2$) used to evaluate the grafting kinetics under different power and concentration conditions. The OPD images are integrated over the region of interest (ROI) in each phase image, leading to the total optical volume (OVD). The particular sequence shown is obtained for the following conditions: 5 mM 4-NBD, 50 μW ($\sim 15 \text{ kW cm}^{-2}$). (B) Evolution of the OVD curves is plotted at several radical precursor concentrations as a function of the excitation energy, indicating that the reaction efficiency is not strongly dependent on the excitation power. The colors indicate the laser fluency: 200 μW ($\sim 60 \text{ kW cm}^{-2}$, blue), 50 μW ($\sim 15 \text{ kW cm}^{-2}$, orange), 12.5 μW ($\sim 4 \text{ kW cm}^{-2}$, yellow) and 3.12 μW ($\sim 1 \text{ kW cm}^{-2}$, purple). (C) Evolution of the grafting efficiency with the precursor concentration (3σ error bars, describing a total of 69 grafting operation).



the excitation beam during the acquisition of the images. An Arduino board is used to manage the acquisition of phase images and control the laser exposition. Aside from this small modification, we use the DIPSi phase imaging module integrated with the grafting setup as described in detail elsewhere.¹⁷ Most of the grafting experiments described in this paper were carried out with a 474 nm pulsed laser (LDH-P-C-470, Picoquant, 40 MHz), except for the wavelength scan experiments, in which a supercontinuum laser (SMHP-40.2-A-PP-RC, Leukos 10 MHz) was used and filtered according to the selected wavelengths indicated in the text. In both cases, the interpulse time (25 ns) leads to diffusive transport over distances ($\sqrt{4Dt_{ip}} \sim 5$ nm) which are very short compared to the laser beam waist (650 ± 30 nm), therefore justifying the treatment of all incident radiation as continuous lasers with the same average power. All power measurements were carried out in the sample focal plane (Ophir NOVA II).

Data analysis

Treatment of the raw speckle pattern deformation is carried out using the demon algorithm, as previously described,^{17,34} implemented in Matlab. All subsequent data treatment was performed in Matlab 2021. In all statistical analysis throughout the paper, we indicate the number of total data points by N and the measurement of standard deviation by σ .

Optical volume evaluation

Based on the deformation of a random interference pattern, we are able to track modifications of the imaging wavefront, and use it to deduce the optical path difference (OPD) distribution. In order to account for the whole grafting zone, we evaluate the optical volume difference (OVD) by integrating over the grafting zone (region of interest, or ROI), as indicated in Fig. 1A:

$$\text{OVD} = \iint_{\text{ROI}} \text{OPD} dx dy$$

The OVD is less sensitive to loss of focus,³⁵ improving the reliability of longer experiments and avoiding artefacts. Under the assumption of an isolated Gaussian object of width σ , the two metrics are related by $\text{OVD} = \text{OPD}_{\text{max}} \sigma^2$. We avoid collecting noise by eliminating all pixels within the ROI which present a signal to noise ratio (SNR) < 1 , the background noise level being estimated in a reference zone ($1.5 \times 1.5 \mu\text{m}^2$) away from the grafting region.

Properties of the grafted layer

The optical properties of the nitrophenyl based grafted layer resulting from diazonium photoreduction were determined in detail elsewhere.¹⁷ In particular, the refractive index of the layer at 633 nm was determined to be 1.68 ± 0.02 , and the molar volume was estimated as 0.35 nm^3 per molecule (or a single layer coverage $\Gamma \approx 4 \times 10^{-10} \text{ mol cm}^{-2}$, taking an average molecule height of 0.8 nm). Such average values, consistent with previous experiments¹⁷ and the literature data,^{36,37} are dependent on the grafted layer density and compacity and

could reasonably vary within 20–30%, leading to a systematic error in the provided calculations. For the sake of clarity, such potential variability is not explicitly included in the error estimation shown in this paper as it only marginally affects the relative values. We however highlight that it should be considered when absolute values are sought or when comparing reactions taking place under drastically different conditions.

Results and discussion

Concentration and power density

Using the described quantitative phase imaging (QPI, Fig. 1A) setup, we conducted a comprehensive quantitative study of surface photografting kinetics of 4-nitrobenzene diazonium (4NBD). As indicated in Fig. 1A, the QPI module enables imaging of the optical phase differences due to local refractive index changes generated by the grafting operation. The photografting kinetics can then be quantitatively evaluated by analysing the temporal evolution of the grafted material optical volume (OVD, an integration of the optical path difference image). Grafting operations carried out at power values between 3.12 and 200 μW ($\sim 1\text{--}60 \text{ kW cm}^{-2}$) at 4NBD radical precursor concentrations in the 0.625–20 mM range reveal a linear evolution of the grafting profiles, with higher photonic fluxes and higher concentrations leading to higher grafting rates (ESI S1†). Fig. 1B shows the grafting evolution at several concentrations as a function of the excitation energy. At higher concentrations and power densities, all grafting curves superpose relatively well, indicating that similar grafting efficiencies are obtained. A small power dependency seems to develop at lower concentrations and excitation powers, which likely results from parasitic weak absorptions from solvent molecules or other low efficiency side reactions. These results suggest that, in the excitation regimes probed here, each arising photon perceives a similar probability of triggering a grafting event, which depends on the availability of 4NBD, pointing towards a quasi-steady state concentration profile, limited by mass transport. These observations are consistent with a previous work,¹⁷ for which pseudo-continuous excitation with a focused laser beam (as done in this paper) at similar laser fluencies was sufficient to completely deplete the radical precursor concentration in the focal spot within a few hundred microseconds.

In this reactant-depleted regime, we expect to observe quite low apparent photonic efficiencies (η^{app} , the ratio between incident photons and grafted molecules), which are evaluated next. Considering the refractive index of the material ($n = 1.68 \pm 0.02$) and its average molecular volume ($V_m = 0.35 \pm 0.05 \text{ nm}^3$), we quantitatively evaluate the grafting rate, using eqn (1):

$$\text{GR}_m = \frac{d\text{OVD}}{dt} \frac{1}{\Delta n} \frac{1}{V_m}. \quad (1)$$

The apparent photonic efficiency is then calculated by taking the ratio between the grafting rate and the number of



arriving photons. At 5 mM, for instance, an OVD evolution of $\sim 8 \times 10^7 \text{ nm}^3$ (6.6×10^8 molecules) is observed after a total excitation energy of $4 \times 10^{-4} \text{ J}$ (9.6×10^{14} photons), leading to an apparent photonic efficiency of $(6.0 \pm 1.3) \times 10^{-7}$ ($N = 12$, 3σ). When considered as a function of the precursor concentration, this quantity varies linearly, in accordance with the quasi-steady state diffusion profile. The apparent photonic efficiencies reach $\sim (2.0 \pm 0.4) \times 10^{-6}$ ($N = 14$, 3σ) for 20 mM diazonium solution, which is a few orders of magnitude below the efficiencies previously observed in the absorption-limited grafting regime obtained at low laser fluencies,¹⁷ again supporting the mass transport limitation regime.

The observed molar grafting rates (at most $13.5 \times 10^{-16} \text{ mol s}^{-1}$) are also consistently below the maximal diffusional limit ($\phi_{\text{max}} \sim 10^{-14} \text{ mol s}^{-1}$ for a grafting zone of $\sim 1 \mu\text{m}$; calculation details are shown in ESI S2†), which is the maximal rate for a diffusion limited process in the absence of side reactions. These results suggest that a competition exists between the grafting process and radical reactions taking place in solution, such as radical–radical dimerization.

It is useful to compare this quantitative analysis to the molar absorptivity of the diazonium salt solution, providing insight into the activation mechanism. Surprisingly, UV/vis absorption spectra (ESI Section S3†) reveal very weak molar absorption coefficients in the excitation wavelength ($\epsilon_{474 \text{ nm}} < 100 \text{ M}^{-1} \text{ cm}^{-1}$), prompting a more quantitative analysis of the photografting mechanism. Photoactivation of diazonium salts has previously been explained on the basis of π – π stacking and the consequent apparition of aggregation induced bands,¹² or in terms of the spontaneous formation of radical cations.³⁸ In our system, however, UV/vis absorption spectra do not provide evidence supporting either of these hypotheses, as they remain invariant when the concentration is varied between 2 mM and 20 mM (ESI Section S3†), suggesting that no aggregation takes place under our photografting conditions, and that no new species seems to be formed.

We investigate the situation by performing a reaction quantum yield estimation. Since low ϵ measurements are relatively imprecise and can be easily confused with the background, the existence of absorption bands in the excitation wavelength was more carefully scrutinized by triggering the diazonium salt formation from its aniline precursor *in situ* (Fig. 2). Considering the aniline absorption as the true background level (at least in the excitation range), this experiment provides evidence for absorption bands associated with the aryl diazonium salts due to the formation of the diazonium salt, univocally supporting its attribution and separation from the background. Following the classical diazotization protocol, we perform the reaction at two concentrations: 25 μM , enabling the high absorption UV bands to be clearly observed; and 5 mM, focusing on the visible wavelength region used to excite the photografting reaction.

The insertion of each 4-nitro-aniline solution in the spectrometer cuvette is followed by the addition of the NaNO_2 diazotization reagent (4 eq. for 25 μM and 1 eq. for 5 mM), leading to the kinetics shown in Fig. 2 (25 μM in the main panels and

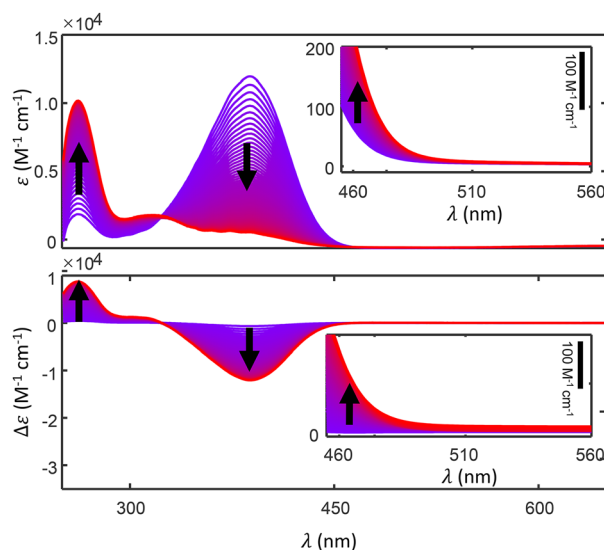


Fig. 2 *In situ* spectral monitoring of diazotization kinetics, from a pH 2 aqueous solution of 25 μM 4-nitro-aniline and 100 μM NaNO_2 , providing evidence for the existence of a positive, albeit weak, absorption band extending into the visible region. $\tau_{\text{acq}} = 1 \text{ min}$. The insets show the corresponding experiments carried out at higher concentrations (5 mM 4-nitro-aniline, 5 mM NaNO_2), enabling the observation of absorption for low molar absorptivity ϵ values.

5 mM in the insets). As can be seen in the main panels, the reaction readily takes place, and its progression is monitored by the decrease in the large absorption peak at 390 nm, with the simultaneous appearance of the characteristic diazonium absorption bands at 260 nm ($\epsilon \sim 10^4 \text{ M}^{-1} \text{ cm}^{-1}$) and 320 nm ($\epsilon \sim 2 \times 10^3 \text{ M}^{-1} \text{ cm}^{-1}$), and of an isosbestic point at 323 nm. A more careful analysis of the excitation wavelength region (474 nm), more easily observed at 5 mM (Fig. 2 insets), reveals a measurable increase of absorption in the excitation region. These results confirm that diazonium salts present a non-zero absorption band in the excitation range, with a molar absorptivity coefficient of $\epsilon_{474 \text{ nm}} \approx 50 \pm 10 \text{ M}^{-1} \text{ cm}^{-1}$ if aniline is considered negligible at this wavelength region. Beer–Lambert's law is then used to give an upper bound for the absorption rate in the vicinity of the surface. Taking as a reference the experiment where 200 μW are concentrated in a focused region of characteristic size 1 μm (laser beam waist) in the presence of 4NBD at a concentration of 5 mM, this analysis suggests that $\sim 3\text{--}9 \times 10^{-16}$ mol of photons per s are absorbed within the surface grafting range ($\sim 20 \text{ nm}$, if a diffusion-limited dimerization reaction is considered as the main deactivation route).

Such a value is comparable with the observed grafting rate ($7 \times 10^{-16} \text{ mol s}^{-1}$), leading to a reaction quantum yield (QY^{r}) close to 1 and suggesting that indeed the absorption is the main pathway leading to the photografting reaction in this diffusion-limited regime. Noteworthy, this calculation does not completely exclude radical propagation pathways (which are likely also active), as it does not consider the local depletion of the reactant due to grafting, helping understand why such a high QY^{r} value is observed.



Wavelength dependency

Our results show that the photografting of diazonium salts can be efficiently triggered at 474 nm, and suggest that even fewer energetic wavelengths could be used, as long as the absorption coefficient is not zero. Indeed, based on the difference spectrum resulting from *in situ* diazotisation (Fig. 2), it should be possible to trigger the reaction with radiation at wavelengths beyond 500 nm, well into the visible region, even if little absorption is observed.

This hypothesis is tested through a wavelength dependency study, using a super continuum laser in association with a series of filters to excite the reaction at different wavelengths while keeping the same power density. The results are shown in Fig. 3. For a total excitation power of 220 μW ($\sim 66 \text{ kW cm}^{-2}$), it is possible to measure significant grafting rates until $\lambda = 516 \text{ nm}$, as predicted. Noteworthy, if higher doses are selected, the grafting rate can also be observed at higher wavelengths, but longer reaction times are required.

Similar results are obtained with control studies carried out with a different diazonium salt presenting a different absorption profile, obtained from the diazotization of *m*-toluidine. Since the corresponding diazonium salt presents a band in the visible range ($\epsilon = 14 \text{ M}^{-1} \text{ cm}^{-1}$, $\lambda_c = 498 \text{ nm}$), a red shift of the grafting reaction onset is expected to occur. Indeed, as shown in ESI Section S4,† even λ as high as 560 nm led to measurable grafting rates, as expected for a direct absorption-based mechanism.

Besides providing insight into the grafting mechanism, this wavelength study also helps rule out a thermal component to the grafting mechanism, as the solvent (water) absorptivity increases with higher wavelengths, and thus should have led to more efficient grafting. We further confirm the lack of thermal effects by attempting to measure the optical index variation (if any) due to temperature differences.

At the maximal irradiation power used in this paper (474 nm, 66 kW cm^{-2}), we were unable to measure any optical path difference (ESI†). Considering the noise level (1 nm peak to peak), the variation of the optical index with temperature,

and the length of the focal spot (defined by the Rayleigh distance), these experiments show that the local temperature variation, if any, is smaller than 2 $^{\circ}\text{C}$, and therefore can be safely neglected.

Our results thus explain why, due to the high local photonic density typically achieved in microscopy settings, even weakly absorbing molecules can lead to photochemical reactions at significant rates. Since diffusive transport is very active at the microscale, heat evacuation operates very efficiently, avoiding associated issues (thermal degradation, side reactions arising from thermodynamic equilibrium displacement, *etc.*). They suggest that weak cumulative or nonlinear effects can lead to an apparent redshift in the activation, without necessarily requiring optical non-linear effects. Several photochemical systems have been shown to display a redshift between the photochemical activity and the absorption spectra,^{39,40} which is often regarded as a positive feature, due to the use of milder wavelengths that avoid side reactions and the use of UV technology.

Our results point out that miniaturization amplifies such effects, enabling photochemical reactions which would be regarded as inactive at mild (visible) spectral regions at larger scales. While low absorption has been previously used to enable subdiffraction fabrication processes,^{41–43} we now suggest that several other photochemical processes could be similarly concerned, highlighting the importance of quantitative and sensitive measurements for understanding local surface modification at the micro and nanoscales.

Influence of side reactions

Although aimed at direct quantification of surface modification reactions, the QPI methodology described in this paper also enables (indirect) quantification of processes taking place in solution, such as the presence of side reactions. Understanding the influence of side effects can be of great importance for designing a grafting operation as, for instance, homogeneous reactions of radicals with the solvent or additives can greatly reduce the grafting rates and efficiency. It is critical to be able to quantify such effects when, for example, organic solvents are used as co-solvents to minimize solubility issues (a rather frequent situation).

We thus consider, as a first example, the influence of dimethylsulfoxide (DMSO) content in the solvent. DMSO contains two methyl groups which are susceptible to hydrogen atom abstraction,⁴⁴ potentially leading to the deactivation of formed aryl radicals and to reduction of the grafting rate.

Indeed, when radicals are generated in the presence of DMSO, hydrogen atom transfer is expected to start a chain of reactions ultimately leading to the deactivation of diazonium salts and the formation of side products, as confirmed by NMR control experiments (ESI S6†).

The effect of the side reactions on the grafting efficacy can be appreciated quantitatively in a series of experiments shown in Fig. 4A, in which the same grafting operation is carried out in mixtures of water and DMSO at different proportions. Starting from an average grafting efficiency of $(5 \pm 1) \times 10^{-7} \text{ (N)}$

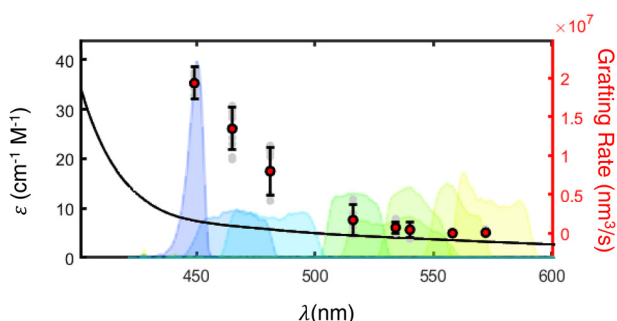


Fig. 3 An action plot comparing the molar absorption coefficient (left axis, black line) and the spectral dependency of the grafting rate at constant incident power (220 μW , $\sim 66 \text{ kW cm}^{-2}$). The graphs in the background indicate the normalized excitation spectra used for each data point.



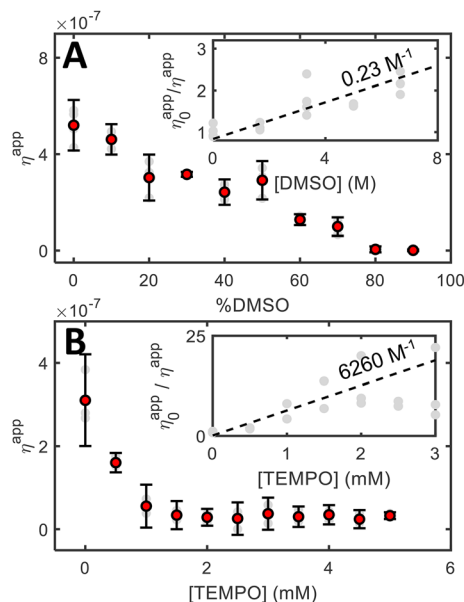


Fig. 4 Influence of the presence of different radical quenchers in the grafting efficiency. (A) As a function of DMSO solvent content, leading to a measurable, but fairly inefficient deactivation (~ 4 M for reducing the grafting rate by 50%). (B) As a function of the TEMPO radical scavenger, leading to an apparent diffusion-limited deactivation dynamics.

$= 4, 3\sigma$) in the absence of DMSO, the grafting efficiency decreases in an approximately linear fashion as the proportion of DMSO is increased, completely vanishing at ~ 80 vol%.

The deactivation efficiency can be more quantitatively analysed in terms of a grafting quenching process, analogously to the Stern–Volmer analysis for fluorescence. Assuming that the radical lifetime is defined by a diffusion-limited dimerization reaction (leading to $\tau_{\text{rad}} \approx 1/k_{\text{diff}} \approx 100$ ns at 5 mM), a modest deactivation rate constant is obtained ($\sim 2 \times 10^6 \text{ M}^{-1} \text{ s}^{-1}$), in orders of magnitude lower than a diffusion-limited rate ($\sim 10^{10} \text{ M}^{-1} \text{ s}^{-1}$). These results suggest that DMSO parasitic reactions do take place, but do not constitute an efficient deactivation pathway. Noteworthy, experiments conducted in the presence of acetonitrile (ACN), another good H^\bullet donor,⁴⁴ yielded qualitatively similar results (grafting rate reduction, difficult grafting at high vol% ACN), but the experiments were perturbed by the solvent volatility, precluding a meaningful quantitative analysis.

We contrast these results with more efficient deactivation reactions specifically targeting radical species, such as deactivation by reaction with a radical scavenger such as (2,2,6,6-tetramethylpiperidin-1-yl)-oxy (TEMPO). In the presence of this molecule, a proportion of the nitrophenyl radicals is expected to form a TEMPO adduct (TEMPO-4NPh) instead of grafting. TEMPO indeed disturbs much more efficiently the grafting rate, as shown in Fig. 4B. The addition of only 1 mM TEMPO to a 5 mM diazonium solution leads to a drastic ($\sim 80\%$) grafting suppression. By performing the same quenching analysis as for DMSO, we obtain a deactivation constant of $\sim 6 \times 10^{10}$

$\text{M}^{-1} \text{ s}^{-1}$, which is consistent with a diffusion-limited deactivation process.

We thus show that quantitative optical monitoring also enables the gathering of indirect information about processes taking place in solution, including deactivation reactions, which enables a much more complete description of the surface modification processes.

Conclusions

In this paper, we have investigated in detail the mechanisms leading to the direct photoactivation of diazonium salts in the visible range by monitoring surface modifications with quantitative phase imaging. We show that direct absorption is the main mechanism driving the surface modification process, enabling grafting rates of $\sim 10^{-16} \text{ mol s}^{-1}$ to be straightforwardly achieved at wavelengths for which the salt presents relatively weak molar absorption coefficients without the need for any additive. We also show that the methodology can be used to (indirectly) evaluate the influence of homogeneous processes which affect the grafting rates, using solvent hydrogen abstraction and radical scavenging reactions as examples. Introducing a grafting inhibition analysis analogous to fluorescence quenching, we quantitatively compare radical deactivation routes and show that radical scavenging can be a fast process operating near the diffusion limit.

We thus quantitatively describe aryldiazonium salts' photo-grafting kinetics as a function of several parameters, enabling the generalization of electrografting methodologies to photochemical routes, while improving both spatial and temporal control of the reaction and the kind of usable substrates (notably nonconductive ones). In the process, we also highlight that high photonic fluxes typically achieved in microscopy setups enable flexibilization of photon absorption criteria for photochemical processes, allowing very weakly absorbing reactants to exhibit significant photochemical activity. Although such conclusions are drawn for the specific case of photografting from diazonium salts, they are expected to hold for other surface modification and other photochemically driven processes, such as photoisomerization and photocatalysis.

Author contributions

BM and MJ performed the experiments, BM and VB analysed the data, JFA, FM, and VB designed the methodology, FM and VB were responsible for acquiring funding and VB designed the research, wrote the original draft and supervised the research.

Conflicts of interest

There are no conflicts to declare.



Acknowledgements

We gratefully acknowledge support from Agence Nationale de la Recherche (ANR-19-CE09-0013 APMJ). MJ acknowledges NSF funding through the REU Program Modern Optics in the City of Light (award number 1757523). We thank Dr Pascal Berto, Prof. J. C. Lacroix and Dr Sarra G. Derrouich for their helpful discussions.

Notes and references

- 1 Z. Li and K. S. Suslick, *Acc. Chem. Res.*, 2021, **54**, 950–960.
- 2 H. H. Shuai, C. Y. Yang, H. I. C. Harn, R. L. York, T. C. Liao, W. S. Chen, J. A. Yeh and C. M. Cheng, *Chem. Sci.*, 2013, **4**, 3058–3067.
- 3 P.-O. Strale, A. Azioune, G. Bugnicourt, Y. Lecomte, M. Chahid and V. Studer, *Adv. Mater.*, 2016, **28**, 2024–2029.
- 4 G. Liu, S. H. Petrosko, Z. Zheng and C. A. Mirkin, *Chem. Rev.*, 2020, **120**, 6009–6047.
- 5 C. W. Lin, S. Aguilar, E. Rao, W. H. Mak, X. Huang, N. He, D. Chen, D. Jun, P. A. Curson, B. T. McVerry, E. M. V. Hoek, S. C. Huang and R. B. Kaner, *Chem. Sci.*, 2019, **10**, 4445–4457.
- 6 A. Meister, M. Gabi, P. Behr, P. Studer, J. Vörös, P. Niedermann, J. Bitterli, J. Polesel-Maris, M. Liley, H. Heinzelmann and T. Zambelli, *Nano Lett.*, 2009, **9**, 2501–2507.
- 7 M. Yan, J. C. Lo, J. T. Edwards and P. S. Baran, *J. Am. Chem. Soc.*, 2016, **138**, 12692–12714.
- 8 M. R. Heinrich, *Chem. – Eur. J.*, 2009, **15**, 820–833.
- 9 T. Perchyonok, *Radical Reactions in Aqueous Media*, The Royal Society of Chemistry, 2009.
- 10 J. Pinson and F. Podvorica, *Chem. Soc. Rev.*, 2005, **34**, 429–439.
- 11 S. Baranton and D. Bélanger, *J. Phys. Chem. B*, 2005, **109**, 24401–24410.
- 12 M. Busson, A. Berisha, C. Combella, F. Kanoufi and J. Pinson, *Chem. Commun.*, 2011, **47**, 12631–12633.
- 13 C. Combella, F. Kanoufi, J. Pinson and F. I. Podvorica, *J. Am. Chem. Soc.*, 2008, **130**, 8576–8577.
- 14 T. Cottineau, M. Morin and D. Bélanger, *RSC Adv.*, 2013, **3**, 23649–23657.
- 15 M. C. Rodríguez González, A. Brown, S. Eyley, W. Thielemans, K. S. Mali and S. de Feyter, *Nanoscale*, 2020, **12**, 18782–18789.
- 16 J. Greenwood, T. H. Phan, Y. Fujita, Z. Li, O. Ivasenko, W. Vanderlinden, H. van Gorp, W. Frederickx, G. Lu, K. Tahara, Y. Tobe, H. Uji-i, S. F. L. Mertens and S. de Feyter, *ACS Nano*, 2015, **9**, 5520–5535.
- 17 V. Brasiliense, J.-F. Audibert, T. Wu, G. Tessier, P. Berto and F. Miomandre, *Small Methods*, 2022, 2100737.
- 18 M. M. Chehimi, A. Lamouri, M. Picot and J. Pinson, *J. Mater. Chem. C*, 2014, **2**, 356–363.
- 19 L. Hirt, R. R. Grüter, T. Berthelot, R. Cornut, J. Vörös and T. Zambelli, *RSC Adv.*, 2015, **5**, 84517–84522.
- 20 M. Hirtz, S. Varey, H. Fuchs and A. Vijayaraghavan, *ACS Appl. Mater. Interfaces*, 2016, **8**, 33371–33376.
- 21 C. Cougnon, F. Gohier, D. Belanger and J. Mauzeroll, *Angew. Chem., Int. Ed.*, 2009, **48**, 4006–4008.
- 22 J. Azevedo, L. Fillaud, C. Bourdillon, J. M. Noël, F. Kanoufi, B. Jousselme, V. Derycke, S. Campidelli and R. Cornut, *J. Am. Chem. Soc.*, 2014, **136**, 4833–4836.
- 23 M. Bouriga, M. M. Chehimi, C. Combella, P. Decorse, F. Kanoufi, A. Deronzier and J. Pinson, *Chem. Mater.*, 2013, **25**, 90–97.
- 24 A. Garcia, N. Hanifi, B. Jousselme, P. Jégou, S. Palacin, P. Viel and T. Berthelot, *Adv. Funct. Mater.*, 2013, **23**, 3668–3674.
- 25 R. Ahmad, L. Boubekeur-Lecaque, M. Nguyen, S. Lau-Truong, A. Lamouri, P. Decorse, A. Galtayries, J. Pinson, N. Felidj and C. Mangeney, *J. Phys. Chem. C*, 2014, **118**, 19098–19105.
- 26 Y. Luo, Y. Xiao, D. Onidas, L. Iannazzo, M. Ethève-Quelquejeu, A. Lamouri, N. Féridj, S. Mahouche-Chergui, T. Brulé, N. Gagey-Eilstein, F. Gazeau and C. Mangeney, *Chem. Commun.*, 2020, **56**, 6822–6825.
- 27 S. Betelu, I. Tijunelyte, L. Boubekeur-Lecaque, I. Ignatiadis, J. Ibrahim, S. Gaboreau, C. Berho, T. Toury, E. Guenin, N. Lidgi-Guigui, N. Féridj, E. Rinnert and M. L. D. la Chapelle, *J. Phys. Chem. C*, 2016, **120**, 18158–18166.
- 28 V.-Q. Nguyen, Y. Ai, P. Martin and J.-C. Lacroix, *ACS Omega*, 2017, **2**, 1947–1955.
- 29 P. Bléteau, M. Bastide, S. Gam-Derouich, P. Martin, R. Bonnet and J.-C. Lacroix, *ACS Appl. Nano Mater.*, 2020, **3**, 7789–7794.
- 30 S. Bouden, J. Pinson and C. Vautrin-UI, *Electrochem. Commun.*, 2017, **81**, 120–123.
- 31 L. Pichereau, C. Gautier and T. Breton, *J. Mater. Chem. C*, 2022, 7111–7118.
- 32 N. Marshall, A. Rodriguez and S. Crittenden, *RSC Adv.*, 2018, **8**, 6690–6698.
- 33 A. Sinitskii, A. Dimiev, D. A. Corley, A. A. Fursina, D. V. Kosynkin and J. M. Tour, *ACS Nano*, 2010, **4**, 1949–1954.
- 34 P. Berto, H. Rigneault and M. Guillon, *Opt. Lett.*, 2017, **42**, 5117–5120.
- 35 S. Khadir, D. Andrén, P. C. Chaumet, S. Monneret, N. Bonod, M. Käll, A. Sentenac and G. Baffou, *Optica*, 2020, **7**, 243.
- 36 T. Menanteau, E. Levillain and T. Breton, *Chem. Mater.*, 2013, **25**, 2905–2909.
- 37 P. A. Brooksby and A. J. Downard, *Langmuir*, 2004, **20**, 5038–5045.
- 38 S. Witzel, M. Hoffmann, M. Rudolph, M. Kerscher, P. Comba, A. Dreuw and A. S. K. Hashmi, *Cell Rep. Phys. Sci.*, 2021, **2**(2), 100325.
- 39 I. M. Irshadeen, S. L. Walden, M. Wegener, V. X. Truong, H. Frisch, J. P. Blinco and C. Barner-Kowollik, *J. Am. Chem. Soc.*, 2021, **143**, 21113–21126.



- 40 I. M. Irshadeen, K. de Bruycker, A. S. Micallef, S. L. Walden, H. Frisch and C. Barner-Kowollik, *Polym. Chem.*, 2021, **12**, 4903–4909.
- 41 M. T. Do, T. T. N. Nguyen, Q. Li, H. Benisty, I. Ledoux-Rak and N. D. Lai, *Opt. Express*, 2013, **21**, 20964–20973.
- 42 F. Mao, Q. C. Tong, D. T. T. Nguyen, A. T. Huong, R. Odessey, F. Saudrais and N. D. Lai, *Advanced Fabrication Technologies for Micro/Nano Optics and Photonics X*, SPIE, 2017, vol. 10115, p. 1011509.
- 43 T. H. Au, A. Perry, J. Audibert, D. T. Trinh, D. B. Do, S. Buil, X. Quélin, J. P. Hermier and N. D. Lai, *Sci. Rep.*, 2020, **10**, 4843.
- 44 F. M'Halla, J. Pinson and J. M. Savéant, The Solvent as H-Atom Donor in Organic Electrochemical Reactions. Reduction of Aromatic Halides, *J. Am. Chem. Soc.*, 1980, **102**(12), 4120–4127.
- 45 T. Wu, M. Guillon, C. Gentner, H. Rigneault, G. Tessier, P. Bon and P. Berto, 3D nanoparticle superlocalization with a thin diffuser, *Opt. Lett.*, 2022, **47**(12), 3079–3082.

